Two-Dimensional Model for Proton Exchange Membrane Fuel Cells

Vladimir Gurau, Hongtan Liu, and Sadik Kakaç
Dept. of Mechanical Engineering, University of Miami, Coral Gables, FL 33124

A 2-D mathematical model for the entire sandwich of a proton-exchange membrane fuel cell including the gas channels was developed. The self-consistent model for porous media was used for the equations describing transport phenomena in the membrane, catalyst layers, and gas diffusers, while standard equations of Navier-Stokes, energy transport, continuity, and species concentrations are solved in the gas channels. A special handling of the transport equations enabled us to use the same numerical method in the unified domain consisting of the gas channels, gas diffusers, catalyst layers and membrane. It also eliminated the need to prescribe arbitrary or approximate boundary conditions at the interfaces between different parts of the fuel cell sandwich. By solving transport equations, as well as the equations for electrochemical reactions and current density with the membrane phase potential, polarization curves under various operating conditions were obtained. Modeling results compare very well with experimental results from the literature. Oxygen and water vapor mole fraction distributions in the coupled cathode gas channel-gas diffuser were studied for various operating current densities. Liquid water velocity distributions in the membrane and influences of various parameters on the cell performance were also obtained.

Introduction

One of the most challenging problems in fuel cells modeling is the possibility to simulate, rather than prescribe or guess, the concentration variations along the interface between the gas diffusers and catalyst layers. This is a major problem, since the distribution of the reactant concentrations along the electrodes is needed to calculate the transfer currents in electrochemical cells. In the particular case of a PEM fuel cell, this phenomenon is related to the gas transport in the coupled domain of a gas channel-gas diffuser-catalyst layer, and the inability to solve the transport equations in this heterogeneous domain apparently has been the main drawback in simulating reactant distributions. A mathematical model together with a numerical procedure featuring this ability would represent a significant step in simulating transport phenomena and performance of PEM fuel cells.

In their study, Ridge et al. (1989), Verbrugge and Hill (1990a,b), Bernardi and Verbrugge (1991, 1992), and Springer et al. (1991) treated 1-D models of the same problem which provided useful information for further development of the 2-D models.

The 2-D models published so far are mostly concerned with the transport phenomena in the domains consisting of the membrane, catalyst layers, and gas diffusers, while the concentrations/partial pressures in the gas channels are assumed more or less arbitrarily, or averaged values are used as boundary conditions at the interface with the gas diffusers. The work of Singh et al. (1996) assumed linear variations of the chemical species at the gas channel-gas diffuser interfaces, and the developed model describes phenomena exclusively in the membrane-catalyst layers-gas diffusers. Fuller and Newman (1993) solved for the transport across the fuel cell sandwich at certain locations along the gas channel and thereafter integrated in the second direction, while the gas outside the gas diffusers was assumed to be of uniform composition in the direction across the cell. Nguyen and White (1993) used algebraic expressions for the concentrations along the electrodes, while Amphlett et al. (1995), in their modeling of the Ballard IV fuel cell, assumed averaged partial pressures along the gas channels.

Current address of V. Gurau: Energy Partners, 1501 Northpoint Parkway, Suite 102, West Palm Beach, FL 33407.

Table 1. Physical Parameters of Fuel Cell Elements

Gas channel length, 7.62×10^{-2} m
Gas channel width, $D = 7.62\times10^{-4}$ m
Gas diffuser width, 2.54×10^{-4} m
Catalyst layer width, $D_{cl} = 0.287\times10^{-4}$ m
Membrane width, $L = 2.3\times10^{-4}$ m (Bernardi and Verbrugge, 1991)
Gas diffuser porosity, $\epsilon = 0.4$
Membrane porosity, $\epsilon_m = 0.28$ (Bernardi and Verbrugge, 1991)
Vol. fraction memb. in catalyst layer, $\epsilon_{mc} = 0.5$ (Bernardi and Verbrugge, 1991)
Permeability to air of gas diffuser, $k = 1.76\times10^{-11}$ m^2
Thermal conduc. of graphite matrix of gas diffuser, $k_{gr} = 150.6$ W·m^{-1}·K^{-1}
Hydraulic permeability of memb., $k_p = 1.58\times10^{-18}$ m^2 (Bernardi and Verbrugge, 1991)
Electrokinetic permeab. of memb., $k_\Phi = 1.13\times10^{-19}$ m^2 (Bernardi and Verbrugge, 1991)
Thermal conduc. of dry memb., $k_{m,\mathrm{dry}} = 100$ W·m^{-1}·K^{-1}
Fixed charged site concen. in memb., $c_f = 1.2\times10^3$ mol·m^{-3} (Bernardi and Verbrugge, 1991)
Charge of sulfonate site in memb., $z_f = -1$
Ref. exch. current density times area, $aj_0^{\mathrm{ref}} = 5\times10^2$ A·m^{-3} (Bernardi and Verbrugge, 1991)
Cathodic transfer coeff. for cathode, $\alpha_c = 2$ (Bernardi and Verbrugge, 1991)

In reality, the concentrations along the gas channels-gas diffusers-catalyst layers will vary due to diffusion-convection transport and electrokinetics in the catalyst layers. These distributions will depend therefore on the gas/medium properties, as well as on the reaction rates. These latter ones are in turn functions of the reactant concentrations and an iterative procedure would be required to predict them. A proper description of the species concentration distribution would involve the use of the 2-D momentum equations in the coupled gas channel-gas diffuser-catalyst layer domain. Together with the continuity and species concentration equations (Stefan-Maxwell), equations describing the electrochemical reactions have to be also part of the system. These latter ones are coupled with the transport equations in membrane via electroosmotic terms. The only independent variables for constant geometry and material properties are the mass-flow rates, temperatures, humidities, and the pressures of the gas mixtures at the gas channel inlets, the external circuit resistance, and the temperature of the heating (cooling) agent, the last one having influence on the electrochemical reactions via Arrhenius type terms. These are actually the only parameters that can be controlled in laboratory experiments or other fuel cell applications.

Table 2. Physical Parameters of the Fluids: Base Case Conditions

Air inlet temperature, $T_i = 353$ K
Air inlet pressure, $p_i = 3$ atm
Air inlet velocity, $U_i = 0.35$ m·s^{-1}
Air viscosity, $\mu = 1.85\times10^{-5}$ kg·m^{-1}·s^{-1}
Air thermal conductivity, $k = 2.5\times10^{-2}$ W·m^{-1}·K^{-1}
Molecular mass of air, 29×10^{-3} kg·mol^{-1}
Molecular mass of oxygen, 32×10^{-3} kg·mol^{-1}
Molecular mass of nitrogen, 28×10^{-3} kg·mol^{-1}
Molecular mass of water, 18×10^{-3} kg·mol^{-1}
Air specific heat at const. pres., $c_p = 1{,}008$ J·kg^{-1}·K^{-1}
Air relative humidity at inlet, 100%
Oxygen/nitrogen ratio in air at inlet, 0.21/0.79
Hydrogen inlet pressure, $p_i = 1$ atm
Water density, $\rho = 971.1$ kg·m^{-3}
Water viscosity, $\mu = 8.91\times10^{-4}$ kg·m^{-1}·s^{-1}
Water thermal conductivity, $k = 0.6$ W·m^{-1}·K^{-1}
Water specific heat at const. pres., $c_p = 4{,}190$ J·kg^{-1}·K^{-1}
Proton diffusivity in water, $D_{H+} = 4.5\times10^{-9}$ atm m^2·s^{-1} (Bernardi and Verbrugge, 1991)
Critical temperature for oxygen, $T_{cr} = 154.4$ K
Critical pressure for oxygen, $p_{cr} = 49.7$ atm
Critical temperature for nitrogen, $T_{cr} = 126.2$ K
Critical pressure for nitrogen, $p_{cr} = 33.5$ atm
Critical temperature for water, $T_{cr} = 647.3$ K
Critical pressure for oxygen, $p_{cr} = 221.2$ atm

The problem in the coupled domain can be solved without the use of boundary conditions at the interfaces, if all the domain is considered as an entirety. The discretization of the PDEs is done in such a way that the corresponding algebraic equations lead to a correct solution in a domain of large variations of the Peclet number. It is necessary to use proper boundary values for the *parameters*, such as diffusion coefficients, rather than boundary conditions for the *dependent variables* at the interface between layers of different properties. This is the method we have adopted in this work. To the best of our knowledge, there are not any published models that describe the interaction between the gas channels and the rest of the fuel cell sandwich.

Model Description and Assumptions

A typical PEM fuel cell is shown in Figure 1. The collector plates, made of an electrically conductive material, are pro-

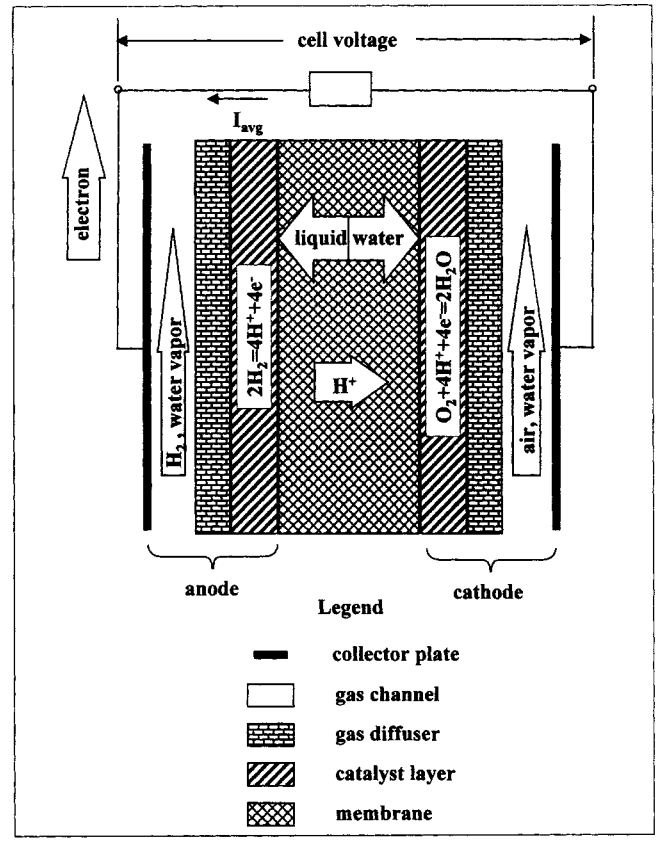

Figure 1. 2-D PEM fuel cell.

vided on both sides with gas channel networks. Between the two collector plates, there are two networks of flow channels, two gas diffusers, two catalyst layers, and the membrane.

The collector plates are in contact with the porous gas diffusers, which in many cases are made of graphite paper or graphite cloth and locally coated with hydrophobic polytetrafluorethylene (PTFE). The transports of the gas mixture components through the pores of the gas diffuser are determined by the momentum transport across the interface between the channel and the gas diffuser, as well as by the concentration and pressure gradients. The graphite matrix of the gas diffusers provides path for the electrons to be transported between the collector plates and the catalyst layers of the MEA.

The MEA assembly is formed by a perfluorosulfonic acid polymer film, called proton exchange membrane (PEM), and two catalyst layers, bounded on each side of the PEM by hot pressing or some other forms of deposition. The PEM is a transparent film with the thickness of some fractions of a millimeter, and a macromolecule having a structural unit formula that enables protons from the sulfonate site to detach and hop from site to site throughout the material. The catalyst layers are made from a mixture of graphite powder, PEM powder and a catalyst, usually platinum, bonded to the gas diffuser.

The hydrogen from the anode gas channels will be transported through the adjacent gas diffuser towards the catalyst layer, where it oxidizes according to the reaction

$$2H_2 \rightarrow 4H^+ + 4e^-$$

Protons are hydrated by water that impregnates the PEM. The liquid water in PEM will be transported due to diffusion, dispersion, pressure gradients, and proton drag. The air mixture in the cathode gas channels will be partially transported through the adjacent gas diffuser towards the catalyst layer, where oxygen will react with protons coming from the anode through the PEM and with the electrons coming from the anode through an external circuit, according to

$$O_2 + 4H^+ + 4e^- \rightarrow 2H_2O$$

The model used here is 2-D, and is presented in Figure 1. It represents a cross-section along one of the cathode channels and contains all fuel cell elements from one collector plate to the other. It is assumed here that the design of the collector plates is such that the anode and cathode gas channels have the same orientation and appear in the same cross-section.

In the model development, the following assumptions are used:

- The gas mixtures are considered to be perfect gases.
- The volume occupied by liquid water in the gas channels coming from the gas diffusers is negligible (in gas channels, only gas mixtures are present).
- The flow is laminar everywhere.
- The gas mixture flows are incompressible.
- Only the steady-state case is considered.
- The gas diffusers, catalyst layers, and the PEM are considered each as isotropic porous media.
- Dilation or contraction of the porous media is neglected.
- The contact electrical losses at the interfaces between different fuel cell elements are neglected.
- The catalyst layers are considered to have vanishing small thickness when the transport equations are solved, but the real values are taken into account when the membrane phase potential and current density are calculated.
- The dispersion of the fluids in the porous media is disregarded at this stage. Its effects can be easily accounted in the general diffusion coefficients.
- The heat generated under reversible conditions is neglected in this work.

Mathematical Model

Our mathematical model uses nondimensional transport equations. Three different domains are considered, corresponding to the phases of the fluid taken into account: the cathode gas channel-gas diffuser-catalyst layer for the air mixture; the cathode gas diffuser-catalyst layer-membrane-anode catalyst layer-gas diffuser for liquid water; the anode gas channel-gas diffuser-catalyst layer for hydrogen.

In the gas channels

The fluid mechanics in the gas channel are described by the continuity and Navier-Stokes equations, which in nondimensional form and under the assumptions mentioned in the previous section become (Kakaç and Yener, 1994)

$$\frac{\partial \bar{u}}{\partial \bar{x}} + \frac{\partial \bar{v}}{\partial \bar{y}} = 0 \tag{1}$$

$$\bar{u}\frac{\partial \bar{u}}{\partial \bar{x}} + \bar{v}\frac{\partial \bar{u}}{\partial \bar{y}} = -\frac{\partial \bar{p}}{\partial \bar{x}} + \frac{1}{Re}\left(\frac{\partial^2 \bar{u}}{\partial \bar{x}^2} + \frac{\partial^2 \bar{u}}{\partial \bar{y}^2}\right) \tag{2}$$

$$\bar{u}\frac{\partial \bar{v}}{\partial \bar{x}} + \bar{v}\frac{\partial \bar{v}}{\partial \bar{y}} = -\frac{\partial \bar{p}}{\partial \bar{y}} + \frac{1}{Re}\left(\frac{\partial^2 \bar{v}}{\partial \bar{x}^2} + \frac{\partial^2 \bar{v}}{\partial \bar{y}^2}\right) \tag{3}$$

where the nondimensional parameters are defined as

$$\bar{u} = \frac{u}{U_i}, \quad \bar{v} = \frac{v}{U_i}, \quad \bar{x} = \frac{x}{D}, \quad \bar{y} = \frac{y}{D},$$

$$\bar{p} = \frac{p - p_i}{\rho_i U_i^2}, \quad Re = \frac{\rho_i U_i D}{\mu}$$

Similarly, the energy equation becomes

$$\bar{u}\frac{\partial \bar{T}}{\partial \bar{x}} + \bar{v}\frac{\partial \bar{T}}{\partial \bar{y}} = \frac{1}{RePr}\left(\frac{\partial^2 \bar{T}}{\partial \bar{x}^2} + \frac{\partial^2 \bar{T}}{\partial \bar{y}^2}\right) \tag{4}$$

where,

$$\bar{T} = \frac{T - T_w}{T_i - T_w} \quad \text{and} \quad Pr = \frac{\mu c_p}{k}$$

The equation for the species concentration is

$$\bar{u}\frac{\partial X_k}{\partial \bar{x}} + \bar{v}\frac{\partial X_k}{\partial \bar{y}} = \frac{1}{ReSc_k}\left(\frac{\partial^2 X_k}{\partial \bar{x}^2} + \frac{\partial^2 X_k}{\partial \bar{y}^2}\right) \tag{5}$$

where X_k stands for the mole fraction of the kth component, and $Sc_k = \mu/\rho D_k$ is the Schmidt number. The diffusion coefficient of the kth component D_k can be expressed in terms of the binary diffusion coefficients as

$$D_k = \frac{1 - \frac{\rho_k}{\rho}}{\sum_{m \neq k} \frac{c}{c_m}\frac{1}{D_{k,m}}} \tag{6}$$

with c_m being the partial molar concentration.

Equation 5 may be solved only for $n-1$ components (water vapor and oxygen in the cathode), the last one for nitrogen coming out from the relation

$$X_n = 1 - \sum_{i=1}^{n-1} X_i \tag{7}$$

In the gas diffusers

The gas diffusers in our virtual fuel cell are made from graphite cloth.

Particular forms of the transport Eqs. 1–5 may be derived for the gas diffusers if their porous nature is taken into account. This is possible if the macroscopic, instead of the microscopic variables are used, and by ensemble or space averaging the terms in the transport equations.

In terms of macroscopic variables, the continuity equation in the porous gas diffuser reads

$$\frac{\partial \bar{q}_x}{\partial \bar{x}} + \frac{\partial \bar{q}_y}{\partial \bar{y}} = 0 \tag{8}$$

where q_x and q_y are the components of the specific discharge ($\mathrm{m \cdot s^{-1}}$).

The macroscopic velocity field in the porous medium is provided by expressions obtained by space averaging the Navier-Stokes equations. The resulting equations are a generalized form of Darcy's law (Dagan, 1989) and in nondimensional form read as (Gurau, 1998)

$$\frac{1}{\epsilon}\left(\bar{q}_x\frac{\partial \bar{q}_x}{\partial \bar{x}} + \bar{q}_y\frac{\partial \bar{q}_x}{\partial \bar{y}}\right) = -\epsilon\frac{\partial \bar{P}}{\partial \bar{x}} + \frac{1}{Re}r^{(2)}\left(\frac{\partial^2 \bar{q}_x}{\partial \bar{x}^2} + \frac{\partial^2 \bar{q}_x}{\partial \bar{y}^2}\right) - \epsilon\frac{\mu}{k}\cdot\bar{q}_x\frac{D}{\rho_i U_i} \tag{9}$$

$$\frac{1}{\epsilon}\left(\bar{q}_x\frac{\partial \bar{q}_y}{\partial \bar{x}} + \bar{q}_y\frac{\partial \bar{q}_y}{\partial \bar{y}}\right) = -\epsilon\frac{\partial \bar{P}}{\partial \bar{y}} + \frac{1}{Re}r^{(2)}\left(\frac{\partial^2 \bar{q}_y}{\partial \bar{x}^2} + \frac{\partial^2 \bar{q}_y}{\partial \bar{y}^2}\right) - \epsilon\frac{\mu}{k}\cdot\bar{q}_y\frac{D}{\rho_i U_i} \tag{10}$$

with the last terms in Eqs. 9 and 10 standing for the average drag force exerted by the fluid on the solid surface per unit volume of medium, k being the permeability of the gas mixtures in the graphite porous medium ($\mathrm{m^2}$), and ϵ, being the porosity. When $r^{(2)} = 1$, Eqs. 9 and 10 turn into Brinkman's equations. Dagan (1979) showed that $r^{(2)} \gg 1$, and the relationship for $r^{(2)}$ can be estimated as

$$r^{(2)} = 2.25\frac{(1-\epsilon)^2}{\epsilon^2} \tag{11}$$

At this stage, it is clear to see the similarity between Eqs. 2–3 and Eqs. 9–10. This enables us to consider the whole domain (channel + gas diffuser) as an entirety, if in the numerical program the extra body forces are taken into account for the gas diffuser subdomain. When the flow field is obtained numerically, one has to remember that the values of the velocities in the porous gas diffuser stand for the specific discharge. This is reasonable, since q appears in the experimental context in a natural manner when measuring the outflow from a porous laboratory column.

It is important to note that the average viscous stress terms in Eqs. 9 and 10 may be neglected for slow varying velocity field in space, yielding Darcy's equations, but have to be taken into account if the macroscopic velocity varies rapidly in space, as in the case of the boundary between a porous medium and a channel (Dagan, 1989). In such cases, a thin layer of the order of the pore scale is formed, where the velocity drops very fast (as will be seen in Figure 3). The Darcy's law is not applicable in this layer; therefore, special boundary conditions would have to be used to connect the flow field in the channel (described by Navier-Stokes equations) to the flow in the porous medium (described by Darcy's law). Our way to solve this problem, as we showed, avoids using boundary conditions and treats the whole domain as an entirety.

In the gas diffuser layers, energy is transported by diffusion and locally by convection in the fluid phase and by conduction in the solid matrix of the porous graphite cloth.

For such a porous medium, the energy equation can be obtained by ensemble averaging the microscopic energy equations in the fluid and solid phase, respectively, and adding them up neglecting the heat generation by viscous dissipation. To define the resulting effective macroscopic heat conductivity, different models of porous media are available in the literature (Dagan, 1989). In the context of these models, the effective conductivity is a function of the fluid phase and solid matrix conductivities. The most suitable model for the graphite cloth gas diffuser is believed to be the self-consistent approximation in which the conductivity of the fictitious homogeneous matrix is taken to be equal to the conductivity of the graphite fibers. This porous medium model is equivalent to the model of a medium in which spherical inclusions filled with fluid are surrounded by solid shells. In this context, the effective macroscopic thermal conductivity k_{eff} is given by the formula

$$k_{\mathrm{eff}} = -2k_{gr} + \frac{1}{\frac{\epsilon}{2k_{gr} + k_{\mathrm{gas}}} + \frac{1-\epsilon}{3k_{gr}}} \tag{12}$$

where k_{gr} and k_{gas} are the thermal conductivities ($\mathrm{W \cdot m^{-1} \cdot K^{-1}}$) of the graphite solid matrix and of the gas mixture, re-

spectively. The energy transport equation for the gas diffusers, in nondimensional form will be therefore (Dagan, 1989; Gurau, 1998)

$$\frac{1}{\epsilon}\left(\bar{q}_x\frac{\partial\bar{T}}{\partial\bar{x}}+\bar{q}_y\frac{\partial\bar{T}}{\partial\bar{y}}\right)=\frac{1}{RePr}\left(\frac{\partial^2\bar{T}}{\partial\bar{x}^2}+\frac{\partial^2\bar{T}}{\partial\bar{y}^2}\right) \tag{13}$$

where

$$Pr=\frac{c_p\mu}{k_{\text{eff}}}$$

c_p standing for the specific heat ($J\cdot kg^{-1}\cdot K^{-1}$) of the gas mixture at constant pressure. The variables in Eq. 13 have been nondimensionalized in the same manner like before. Again, one should notice the similarity between Eqs. 4 and 13.

The chemical species in the gas mixtures will be transported by diffusion and locally by convection. The effective macroscopic diffusion coefficient for the kth component in the frame of the adopted porous medium model will be (Dagan, 1989)

$$\begin{aligned} D_{\text{eff},k}&=\frac{3\epsilon-1}{2\epsilon}D_k \quad \text{if } \epsilon>1/3\\ D_{\text{eff},k}&=0. \quad\quad\quad\quad \text{if } \epsilon\le 1/3\end{aligned} \tag{14}$$

where D_k is the microscopic diffusion coefficient for the kth species ($m^2\cdot s^{-1}$), defined by Eq. 6. The transport equation for the chemical species in nondimensional form will become (Gurau, 1998)

$$\frac{1}{\epsilon}\left(\bar{q}_x\frac{\partial X_k}{\partial\bar{x}}+\bar{q}_y\frac{\partial X_k}{\partial\bar{y}}\right)=\frac{\epsilon}{ReSc_k}\left(\frac{\partial^2X_k}{\partial\bar{x}^2}+\frac{\partial^2X_k}{\partial\bar{y}^2}\right) \tag{15}$$

where Schmidt number is defined in terms of the effective macroscopic diffusion coefficient given by Eq. 14

$$Sc_k=\frac{\mu}{\rho D_{\text{eff},k}}$$

Equation 15 is nondimensionalized in the same manner like Eq. 8 and is similar to it.

In the membrane

The subjects of the transport equations in the porous membrane are variables related to water flow; therefore, similar equations like the ones developed for the gas diffusers may apply, if the proper parameters for water are plugged in. A different form of the momentum transport equations, containing source terms accounting for electroosmotic forces has to be used here. In nondimensional form, these equations read (Gurau, 1998)

$$\frac{1}{\epsilon_m}\left(\bar{q}_x\frac{\partial\bar{q}_x}{\partial\bar{x}}+\bar{q}_y\frac{\partial\bar{q}_x}{\partial\bar{y}}\right)=-\epsilon_m\frac{\partial\bar{P}}{\partial\bar{x}}+\frac{1}{Re}r^{(2)}\left(\frac{\partial^2\bar{q}_x}{\partial\bar{x}^2}+\frac{\partial^2\bar{q}_x}{\partial\bar{y}^2}\right)-\epsilon_m\frac{\mu}{k_p}\cdot\bar{q}_x\frac{D}{\rho_iU_i}+\frac{k_\phi}{k_p}z_fc_fF\frac{\partial\phi}{\partial\bar{x}}\frac{1}{\rho U_i^2L} \tag{16}$$

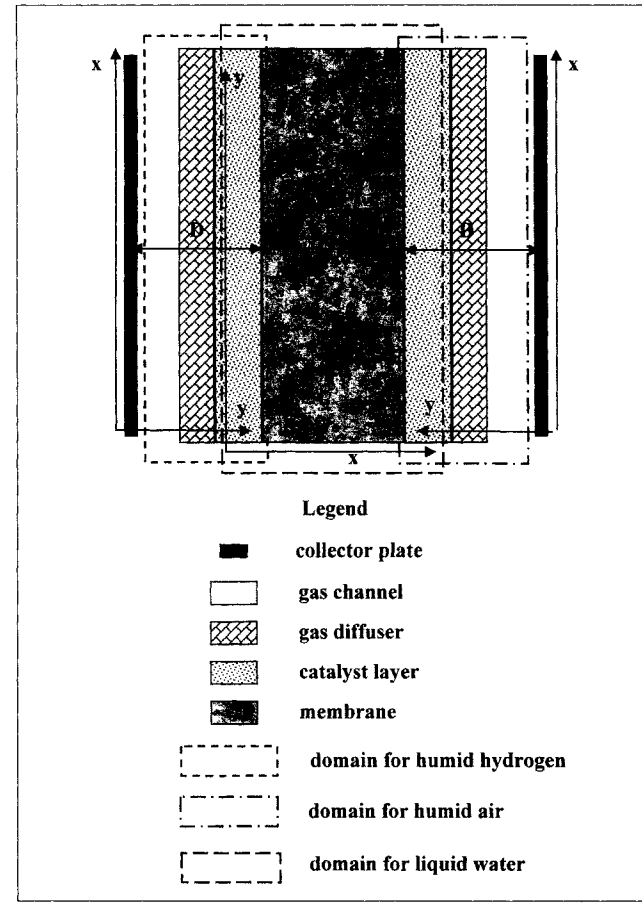

Figure 2. Geometry, coordinate axes, boundary types and characteristic dimensions of the three domains.

$$\frac{1}{\epsilon_m}\left(\bar{q}_x\frac{\partial\bar{q}_y}{\partial\bar{x}}+\bar{q}_y\frac{\partial\bar{q}_y}{\partial\bar{y}}\right)=-\epsilon_m\frac{\partial\bar{P}}{\partial\bar{y}}+\frac{1}{Re}r^{(2)}\left(\frac{\partial^2\bar{q}_y}{\partial\bar{x}^2}+\frac{\partial^2\bar{q}_y}{\partial\bar{y}^2}\right)-\epsilon_m\frac{\mu}{k_p}\cdot\bar{q}_y\frac{D}{\rho_iU_i}+\frac{k_\phi}{k_p}z_fc_fF\frac{\partial\phi}{\partial\bar{y}}\frac{1}{\rho U_i^2L} \tag{17}$$

where k_ϕ stands for the electrokinetic permeability (m^2), k_P for the hydraulic permeability (m^2), z_f for the charge number of the fixed to the backbone polymer chain sulfonic acid ions, c_f for the concentration of the sulfonic ions ($mol\cdot m^{-3}$), F is the Faraday number (96.487 C/mol), ϕ is the potential in the membrane phase (V), ϵ_m is the membrane porosity, and L is the thickness (m) of the membrane (see Figure 2). Equations 16 and 17 represent a generalized form of the Schlögl's equations.

The transport of the hydrated protons is governed by an equation similar to Eq. 15, with an extra term accounting for migration

$$\frac{1}{\epsilon_m}\left(\bar{q}_x\frac{\partial X_{H^+}}{\partial\bar{x}}+\bar{q}_y\frac{\partial X_{H^+}}{\partial\bar{y}}\right)=\frac{\epsilon_m}{ReSc_{H^+}}\left(\frac{\partial^2X_{H^+}}{\partial\bar{x}^2}+\frac{\partial^2X_{H^+}}{\partial\bar{y}^2}\right)+\epsilon_mz_{H^+}X_{H^+}\frac{F}{RT}D_{\text{eff},H^+}\left(\frac{\partial^2\phi}{\partial x^2}+\frac{\partial^2\phi}{\partial y^2}\right)\frac{1}{U_iL} \tag{18}$$

The energy equation is similar to Eq. 13 with a new source term of Joule heating

$$\frac{1}{\epsilon_m}\left(\bar{q}_x\frac{\partial\bar{T}}{\partial\bar{x}}+\bar{q}_y\frac{\partial\bar{T}}{\partial\bar{y}}\right)=\frac{1}{RePr}\left(\frac{\partial^2\bar{T}}{\partial\bar{x}^2}+\frac{\partial^2\bar{T}}{\partial\bar{y}^2}\right)+\frac{i^2}{\sigma_m}\frac{L}{U_i\rho_i c_p T_i} \tag{19}$$

and the effective conductivity given by Eq. 14, with k_{gr} replaced by $k_{m,\mathrm{dry}}$ and k_{gas} by $k_{w,l}$.

In Eq. 19, i is the modules of the membrane phase current density ($\mathrm{A\cdot m^{-2}}$) vector, and σ_m is the ionic conductivity ($\Omega^{-1}\cdot\mathrm{m}^{-1}$).

For the membrane phase potential, the following equation applies

$$\frac{\partial}{\partial x}\left(\sigma_m\frac{\partial\phi}{\partial x}\right)+\frac{\partial}{\partial y}\left(\sigma_m\frac{\partial\phi}{\partial y}\right)=0 \tag{20}$$

and the membrane phase current density satisfies

$$i_x=-\sigma_m\frac{\partial\phi}{\partial x}$$
$$i_y=-\sigma_m\frac{\partial\phi}{\partial y} \tag{21}$$

In the catalyst layers

Continuity and Eqs. 16 and 17 apply in these regions with the porosity ϵ_m replaced by $\epsilon_m\epsilon_{mc}$, where ϵ_{mc} is the membrane volume fraction in the catalyst layer.

The reactants dissolve in water before they are subjected to the electrochemical reaction. At this stage of our model, we will ignore this phenomenon and will assume that they are transported as components of the gas mixtures. Equations like Eq. 15 will therefore apply with the following source terms

At the anode, the source terms for the hydrogen molecules and protons are

$$-\frac{1}{2F}j_a\frac{D}{U_i c},\qquad \frac{1}{F}j_a\frac{L}{U_i c} \tag{22}$$

At the cathode, the source terms for the oxygen, liquid water and protons are

$$-\frac{1}{4F}j_c\frac{D}{U_i c},\quad \frac{1}{2F}j_c\frac{L}{U_i c},\quad -\frac{1}{F}j_c\frac{L}{U_i c} \tag{23}$$

where the transfer current densities j_a and j_c ($\mathrm{A\cdot m^{-3}}$) are defined by the Butler-Volmer expressions

$$j_a=aj_0^{\mathrm{ref}}\left(\frac{X_{\mathrm{H_2}}}{X_{\mathrm{H_2ref}}}\right)^{1/2}\left[e^{(\alpha_a F/RT)\eta}-\frac{1}{e^{(\alpha_c F/RT)\eta}}\right] \tag{24}$$

$$j_c=aj_0^{\mathrm{ref}}\left(\frac{X_{\mathrm{O_2}}}{X_{\mathrm{O_2ref}}}\right)\left[e^{(\alpha_a F/RT)\eta}-\frac{1}{e^{(\alpha_c F/RT)\eta}}\right] \tag{25}$$

Equation 13 applies with a new source term

$$\frac{1}{\epsilon_m\epsilon_{mc}}\left(\bar{q}_x\frac{\partial\bar{T}}{\partial\bar{x}}+\bar{q}_y\frac{\partial\bar{T}}{\partial\bar{y}}\right)=\frac{1}{RePr}\left(\frac{\partial^2\bar{T}}{\partial\bar{x}^2}+\frac{\partial^2\bar{T}}{\partial\bar{y}^2}\right)+i\eta\frac{D}{U_i\rho_i c_p T_i D_{cl}} \tag{26}$$

where D_{cl} is the thickness of the catalyst layer (m).

The membrane phase potential satisfies the equations

$$\frac{\partial}{\partial x}\left(\sigma_m\frac{\partial\phi}{\partial x}\right)+\frac{\partial}{\partial y}\left(\sigma_m\frac{\partial\phi}{\partial y}\right)=-j_a\quad\text{at anode}$$
$$\frac{\partial}{\partial x}\left(\sigma_m\frac{\partial\phi}{\partial x}\right)+\frac{\partial}{\partial y}\left(\sigma_m\frac{\partial\phi}{\partial y}\right)=-j_c\quad\text{at cathode} \tag{27}$$

The membrane phase current density satisfies

$$\frac{\partial i_x}{\partial x}+\frac{\partial i_y}{\partial y}=j_a\quad\text{at anode}$$
$$\frac{\partial i_x}{\partial x}+\frac{\partial i_y}{\partial y}=j_c\quad\text{at cathode} \tag{28}$$

Besides the equations specified previously, the following additional equations have to be also part of the system:

- The equation of state for the perfect gasses apply in the first and third domains of Figure 2

$$\frac{p}{\rho}=RT \tag{29}$$

where R is the gas constant ($8{,}314\ \mathrm{J\cdot mol^{-1}\cdot K^{-1}}$);

- Springer et al. (1991) present the following empirical expressions to determine the ionic conductivity in a 117 Nafion proton exchange membrane

$$\sigma_m^{\mathrm{ref}}=0.005139\lambda-0.00326\quad\text{if }\lambda\geq 1 \tag{30}$$

where σ_m^{ref} is the reference ionic conductivity at a temperature of 303 K. For values of the membrane water content, λ less than one, the reference ionic conductivity is assumed constant. At other temperatures, it is given by

$$\sigma_m(T)=\sigma_m^{\mathrm{ref}}\exp\left[1{,}268\left(\frac{1}{303}-\frac{1}{T}\right)\right] \tag{31}$$

where temperature is expressed in K. The membrane water content in Eq. 30 is given by the following empirical formula (Springer et al., 1991)

$$\lambda=0.043+17.81a-39.85a^2+36.0a^3\quad\text{for }0<a\leq 1$$
$$\lambda=14+1.4(a-1)\quad\text{for }1\leq a\leq 3 \tag{32}$$

a being the water vapor activity at the cathode gas diffuser-catalyst layer interface assuming equilibrium, given by

$$a = \frac{X_w p}{p^{\text{sat}}} \tag{33}$$

The saturated water partial pressure is expressed by the following empirical equation that fits the tabulated values (Springer et al., 1991)

$$\log_{10} p^{\text{sat}} = -2.1794 + 0.02953T - 9.1837\times10^{-5}T^2 + 1.4454\times10^{-7}T^3 \tag{34}$$

- The temperature dependence of the binary diffusion coefficients is given by Slattery and Bird (1958) (as cited by Bird et al., 1960)

$$pD_{A,B} = a\left(\frac{T}{\sqrt{T_{crA}T_{crB}}}\right)^b (p_{crA}p_{crB})^{1/3} \times (T_{crA}T_{crB})^{5/12}\left(\frac{1}{M_A}+\frac{1}{M_B}\right)^{1/2} \tag{35}$$

where a and b are constants, the pressure is in bar, and the binary diffusion coefficient is in $\text{cm}^2\cdot\text{s}^{-1}$.

- The thermodynamic open circuit potential for the overall reaction is given by

$$E = 1.23 - 0.9\times10^{-3}(T-298) + 2.3\frac{RT}{4F}\log\left(p_{\text{H}_2}^2 p_{\text{O}_2}\right) \tag{36}$$

Examination of Eq. 36 shows a decrease of the open circuit potential with temperature. Experimental results show an opposite effect. This is due to higher exchange current density for oxygen reduction at higher temperature (Parthasarathy et al., 1992). At the present time, we are not aware of any mathematical model to describe this dependency; therefore, we used the empirical results of Parthasarathy et al. (1992) in our formulation. They tabulated values for the open circuit potential as a function of temperature, which can be fitted in the following equation

$$E = 0.0025T + 0.2329 \tag{37}$$

where T is in K.

Boundary conditions

As has been already shown, boundary conditions for the *dependent variables* of the transport equations at the interfaces between different layers of the *same* domain (the notion of *same* or *different* domains are related to Figure 2) are not required. Inlet conditions have to be prescribed at the gas channel entries and boundary conditions at the interface between the gas channels and the plate collectors (solid walls) and at the interfaces between *different* domains. At the gas channel entries, conditions of the first kind have to be prescribed for the gas mixture velocities, pressures, temperatures, and component concentrations. At the interfaces between the gas channels and the plate collectors, boundary conditions of the first kind are prescribed for the gas mixture velocity components (no slip condition) and for the temperature if the temperature of the cooling (heating) agent is known, or boundary conditions of the second kind are prescribed if the wall is adiabatic. At the interfaces between the gas diffusers and the gas channels, the following boundary conditions are assumed for the liquid water velocity components

$$\frac{\partial \bar{q}_x}{\partial \bar{x}} = \frac{\partial \bar{q}_y}{\partial \bar{x}} = 0 \tag{38}$$

Similar boundary conditions are prescribed at the lower and upper boundaries that delimit the membrane

$$\frac{\partial \bar{q}_x}{\partial \bar{y}} = \frac{\partial \bar{q}_y}{\partial \bar{y}} = 0 \tag{39}$$

In the gas diffusers, water vapor is considered to be at equilibrium with the liquid water in the pores not aligned with PTFE. Here also, the liquid water temperature is set equal to the temperature of the gas mixtures.

For the membrane phase potential equation, the boundary conditions are:

$\partial\phi/\partial n = 0$ (no protonic current leaves the domain at the upper and lower limits), where n is the direction perpendicular to the upper and lower boundaries.

$\partial\phi/\partial y = 0$ (no protonic current leaves the domain at the interface between the catalyst layer and the gas diffuser).

No boundary conditions are necessary at the interfaces between the membrane and the catalyst layers, since Eqs. 20 and 27 are coupled over the catalyst layers–membrane domain.

Special care has to be taken for the boundary values of some *parameters*, rather than *dependent variables* at the interfaces between layers of the *same domain* (Patankar, 1980).

Solution Technique

The phenomena in the PEM fuel cell elements are strongly interdependent. To solve equations governing these phenomena in one of the elements requires solving equations in all other elements, including the gas channels. Once the equations in the frame of the mathematical model are established, boundary conditions for the dependent variables at the interface between two elements are required to couple them or, if it is possible, the equations are solved in domains covering more then one fuel cell element without boundary conditions, if the proper parameters corresponding to each element are substituted into the equations. This may be possible if the equations describing some phenomenon in more than one fuel cell element have similar forms and can be solved using the same numerical procedure.

Solving the transport equations over domains covering more than one fuel cell element has to be done carefully. In the gas channels and partially in the gas diffusers, the objects of analysis are gas mixtures, while in the PEM, catalyst layers, and partially in the gas diffuser, it is the liquid water. If the energy equation may be solved over the entire domain covering all the fuel cell elements, the same cannot be said about the continuity, momentum and species conservation equations. Therefore, three different domains are used in our

model (Figure 2). The gas diffusers and catalyst layers belong each to two different domains. The transport equations are solved in their nondimensional form. Nondimensionalization is performed for each different domain, with respect to the dimensions shown in Figure 2. The orientation of the coordinate axes for each domain is also shown in this figure.

The velocity and pressure fields for the gas mixtures are solved first in the coupled gas channel-gas diffuser domains. The composition of the gas mixtures will vary, but we still have considered that the gas mixture parameters, such as gas constants, are fixed. This enables us to solve the flow and pressure fields for the gas mixtures first, and once these fields are found, we proceed to solve for the other dependent variables. The gas species concentrations are dependent on the transfer current densities, therefore, the transport equations for the gas components are solved iteratively, together with the Butler-Volmer Eqs. 24 and 25. After convergence is achieved, one proceeds to solve for the transport equations related to the liquid water flow, for the membrane phase potential and current densities. Since the source terms of the energy equations are functions of the current density for the nonisothermal case, after the latter one is found, one has to return to solve all equations again, except those for the velocity and pressure fields of the gas mixtures. Therefore, a new level of iterations is introduced.

There are generally two ways of solving for the electrochemical cell efficiency: either the operating current density is given and different potential losses are calculated, or the so-called potentiostatic approach is used, when the cell potential is set and the current density is calculated. For a 2-D model, the operating current density is expressed as the average of the current density along the interface between the membrane and the catalyst layer. Even if it is provided as an input datum, it is unclear how the correct distribution of the current density along the membrane-catalyst layer interface could be found when its average value is given. One should remember here that the reactant distributions along the catalyst layer is not known *a priori*. This is the reason for which we chose the following approach: The *total electrode overpotential* is assumed first in Eqs. 24 and 25, then the transfer current densities together with the other unknowns are solved. Once the correct current density is found, the ohmic losses can be calculated, and the cell potential is set as the theoretical potential minus the total electrode overpotential, minus the total ohmic losses. Different values of the *total electrode overpotential* are used until the limiting current density is achieved. If one is interested in how much of the *total* electrode overpotential is represented by the *concentration* overpotential, this latter one can now be expressed in terms of the limiting current.

To solve the transport equations, we developed a numerical program using the SIMPLE algorithm of S. V. Patankar and D. B. Spalding, and described by the former (Patankar, 1980).

At the end of this section, we will discuss the validity of solving transport equations of different forms such as Eqs. 2 and 9, Eqs. 3 and 10, Eqs. 4 and 13, and Eqs. 8 and 15, in a heterogeneous domain considered as an entirety, without using boundary conditions for the dependent variables at the interfaces between layers of different properties. We believe that solving numerically the energy or species concentration equations in a heterogeneous domain is already common practice. Care has to be taken only at the discretization and when assigning values for the general diffusion coefficients at the interfaces and for the source terms. A different problem arises when solving momentum equations such as Eqs. 2 and 9, for example. Indeed, here not only is the domain heterogeneous, but the dependent variables themselves are different. However, if we remember that by definition the microscopic velocity is a limiting case of the macroscopic velocity when the porosity ϵ tends to 1, by describing the heterogeneous domain locally as a function of porosity we find ourselves in a case similar to the ones mentioned above. To support this idea, we remember that researchers, who developed boundary conditions for the momentum equations at the interface between a channel and a porous medium, use both microscopic and macroscopic velocity in the same boundary condition expression (Beavers and Joseph, 1967).

Results and Discussion

Validation of mathematical model

The physical parameters used in this study are listed in Tables 1 and 2, unless specified otherwise. Before discussing any results concerning the performance of the modeled fuel cell, or different vectorial and scalar fields, one should analyze the behavior of the mathematical model in predicting the values of the velocity, temperature, pressure, and component concentrations at the interface between a gas channel and the adjacent porous gas diffuser. Concerning the velocity field in this coupled domain, one should expect a developed field in the channel with velocity vanishing at the solid wall (no slip), a parabolic variation in the cross-section with the maximum value not at the center line of the channel, but shifted towards the interface with the porous medium and a nonzero value (slip condition) at this interface (Beavers et al., 1970). The macroscopic velocity in the porous medium should drop very fast from the interface with the channel in a thin layer of the order of the pore size (Dagan, 1989). The transport beyond this layer should be mainly due to diffusion, but convection may still be present. Figure 3 shows a very good prediction of this behavior. For an inlet axial velocity of 0.35 m/s, the velocity profile in a cross-section at some distance from the inlet presents the characteristics mentioned above with a value of approximately 2 mm/s in the channel at the interface with the porous medium, and a boundary layer of about 0.06 mm inside the porous medium. The maximum velocity is shifted from the center line, a distance of 3% of the channel width.

The pressure field in the coupled cathode gas channel-gas diffuser domain also showed similar characteristics as those predicted by Beavers et al. (1970), with a constant axial pressure gradient and the absence of transverse pressure differences in the channel and porous gas diffuser (Gurau, 1998).

If boundary conditions were to be used for the gas component concentrations at the interface between the channel and the porous medium, they would have read as (Dagan, 1989): $c_{i,ch} = c_{i,pm}$, respectively. Figures 8 and 9, for example, will show the oxygen molar fraction in this coupled domain. The specified condition is fulfilled at the boundary. The profiles in the vicinity of the boundary show that convection is much higher in the channel than in the gas diffuser, where the dif-

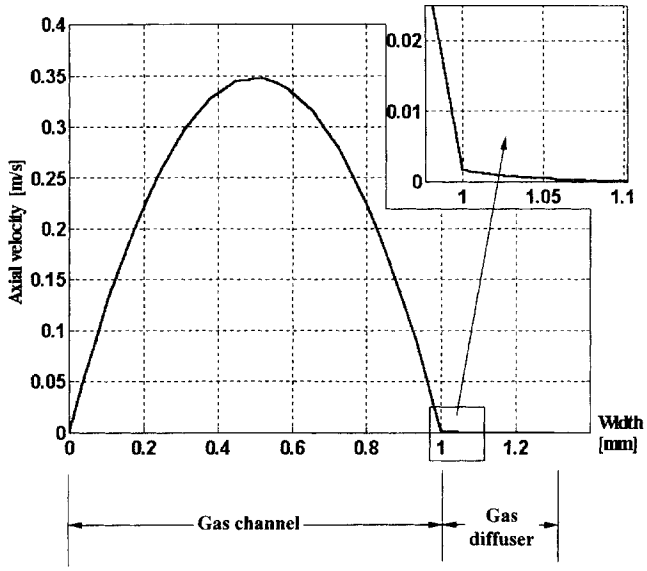

Figure 3. Axial velocity profile across the channel-gas diffuser domain.

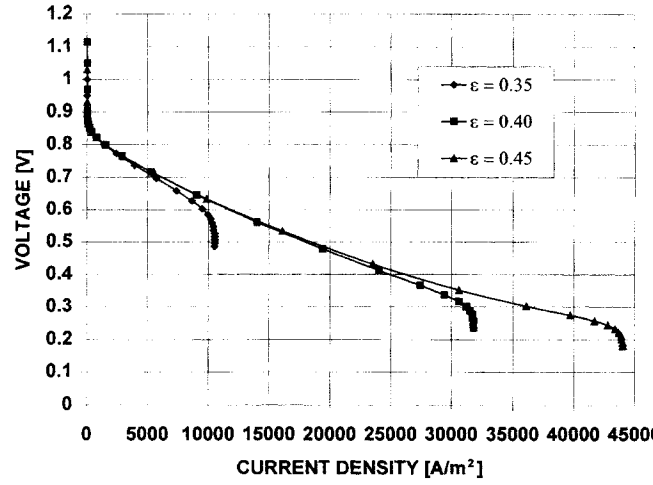

Figure 5. Effect of the gas diffuser porosity on the voltage-current density characteristic.

$U_i = 0.35$ m/s, $T = 353$ K (isothermal case), $X_{w,i}^{\text{sat}} = 0.1579$ (100% humidity).

fusion may be the main transport mean for the gas components.

Figure 4 compares the computed fuel cell characteristic using the present model with the experimental results of Ticianelli et al. (1988), corresponding for a cathode gas channel pressure of 5 atm, an anode gas channel pressure of 3 atm, a cell temperature of 353 K and 20 wt. Pt, 50-nm Pt sputter. It shows a very good agreement between the experimental work and our mathematical model.

Cell performance

In the following paragraphs, the influence of certain parameters on the voltage-current density characteristic are analyzed. The characteristics are compared only to other available computed results, obtained with 1-D numerical models

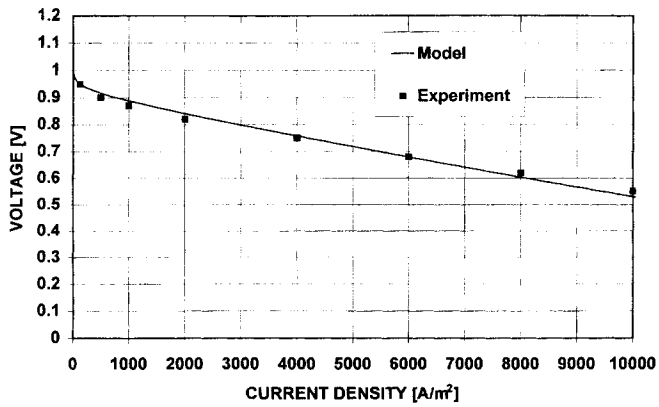

Figure 4 . Mathematical model vs. experimental data of Ticianelli et al. (1988).

Polarization curve corresponding for 5 atm cathode pressure, 3 atm anode pressure, $T = 353$ K, 20 wt. Pt, 50-nm Pt sputter.

(Bernardi and Verbrugge, 1992) but not to any experimental results; therefore, they should be considered mostly qualitative. The computed limiting current densities may be adjusted to the experimental results by means of a proper selection of the reference exchange current density-area product aj_0^{ref}. In our calculations we have chosen the value used by Bernardi and Verbrugge (1991).

Effect of Gas Diffuser Porosity on Cell Performance. Figure 5 shows the cell voltage vs. the operating current density for different values of the gas diffuser porosity ϵ, assuming the isothermal case with the temperature $T = 353$ K, an inlet air velocity ($\text{m}\cdot\text{s}^{-1}$) $U_i = 0.35$ m/s, and the water vapor mole fraction at the gas channel inlet $X_{w,i}^{\text{sat}} = 0.1579$ (100% humidity). For lower values of ϵ, lower values of the limiting current density are found. This phenomenon is due to the limited possibilities of the reactant in the cathode side gas mixture (oxygen) to be transported towards the catalyst layer. Bernardi and Verbrugge (1992) present limiting current density as a function of porosity for three different catalyst layer thicknesses, obtained for their 1-D model. Extrapolating this curve for the catalyst layer thickness used in our model, one may find close values for the limiting current. The slope of the curve is in good agreement with their results as well. Unlike other numerical methods, where the program fails to give results when the limiting current is achieved, the present one is able to predict phenomena even in the region where the concentration overpotentials are predominant.

Effect of the Inlet Air Velocity on Cell Performance. Figure 6 presents the current density for different values of the air velocity at the cathode gas channel entrance, considering the gas diffuser porosity $\epsilon = 0.4$, a constant temperature $T = 353$ K (isothermal case) and the water vapor mole fraction at the cathode gas channel inlet, $X_{w,i}^{\text{sat}} = 0.1579$ (100% humidity). For higher inlet air velocities (higher air mass-flow rates), more oxygen is fed and, therefore, more oxygen is likely to arrive at the catalyst layer, with the result of a higher limiting current density. This is explained by the fact that for the same pressure field, for higher velocities, the axial momentum transfer

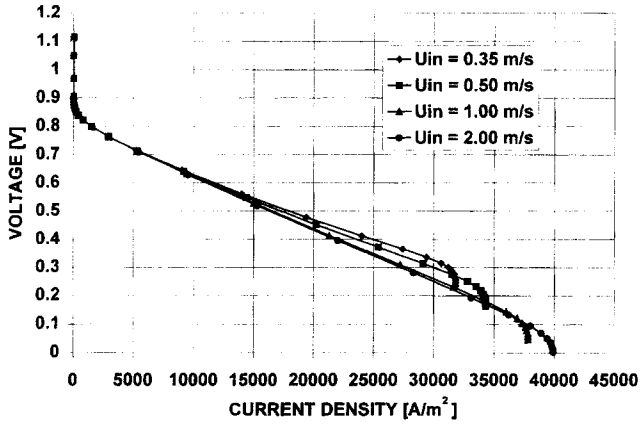

Figure 6. Effect of the air inlet velocity on the voltage-current density characteristic.

$T = 353$ K (isothermal case), $X_{w,i}^{sat} = 0.1579$ (100% humidity), $\epsilon = 0.40$.

across the gas channel-gas diffuser interface becomes more important, with a consequence of more "fresh" air arriving to the catalyst layer. For inlet air velocities higher than approx. 2 m/s, the limiting current becomes constant, which shows that there is a limit effect of the momentum transfer across the gas channel-gas diffuser interface.

Effect of Temperature on Cell Performance. Figure 7 presents the effect of the cell temperature on the voltage-current density characteristic for an inlet air velocity $U_i = 0.35$ m/s, gas-diffuser porosity $\epsilon = 0.4$, and 100% air humidity. Content of water vapor in air at the cathode channel inlet is taken as a function of temperature from available data. Water vapor concentration at the cathode gas-diffuser-catalyst layer interface will determine the liquid water content in the membrane and, therefore, the membrane ionic conductivity with the final effect of better cell performances (higher current densities) at higher temperatures. At higher temperatures, the open circuit potential is higher as well.

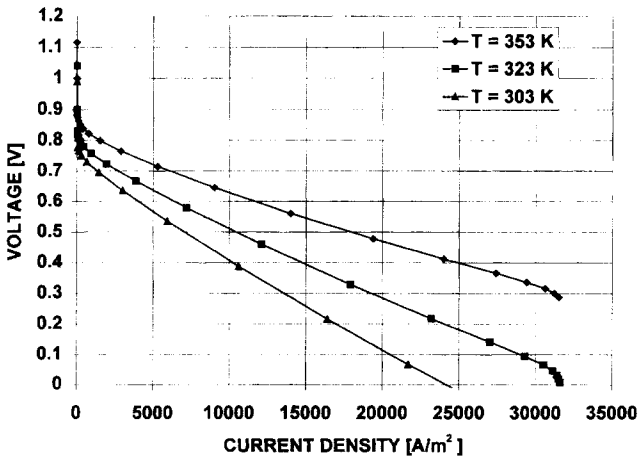

Figure 7. Effect of the cell temperature on the voltage-current density characteristic.

$U_i = 0.35$ m/s, $\epsilon = 0.40$, 100% humidity.

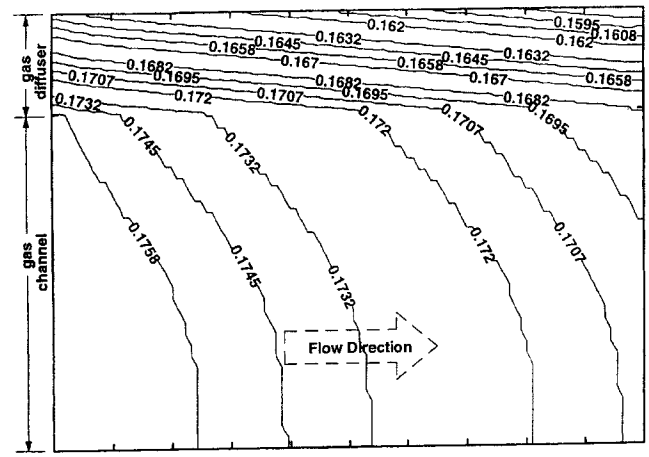

Figure 8. Oxygen mole fraction in the cathode gas channel-gas diffuser domain.

For $I_{avg} = 2.89 \times 10^3$ A/m^2, $U_i = 0.35$ m/s, $T = 353$ K (isothermal case), $X_{w,i}^{sat} = 0.1579$ (100% humidity), $\epsilon = 0.40$. Resulting stoichiometric ratio: $\xi_+ = 25.0$.

Oxygen mole fraction field in the cathode gas channel-gas diffuser coupled domain

Figures 8 and 9 show the oxygen mole fraction field in the coupled cathode gas channel-gas diffuser domain for the base case conditions (isothermal case) and two different operating current densities. The oxygen is consumed in the catalyst layer. The oxygen consumption is higher for higher operating current densities. In Figure 9, where the operating current density is the limiting current, the rate of oxygen depletion is much higher than in Figure 8. Although the rate of oxygen depletion is higher at the left side of the catalyst layer-gas diffuser interface, the oxygen concentration is lower in the right side. This phenomenon is explained by the convective transport in gas diffuser. The corresponding stoichiometric ratios are calculated as the ratio between the average oxygen

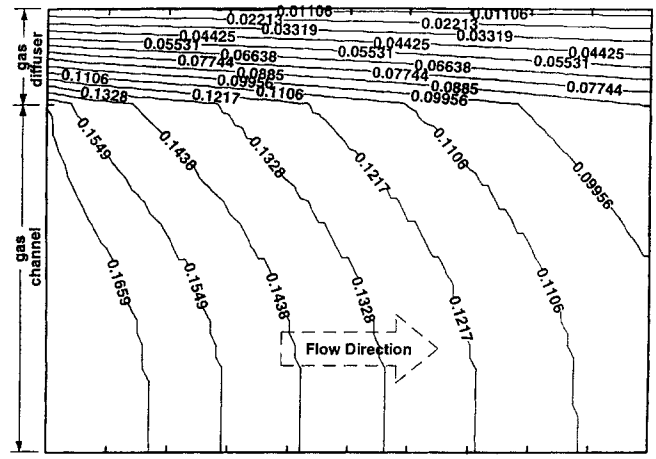

Figure 9. Oxygen mole fraction in the cathode gas channel-gas diffuser domain.

For $I_{avg} = 3.18 \times 10^4$ A/m^2 (limiting current), $U_i = 0.35$ m/s, $T = 353$ K (isothermal case), $X_{w,i}^{sat} = 0.1579$ (100% humidity), $\epsilon = 0.40$. Resulting stoichiometric ratio: $\xi_+ = 2.28$.

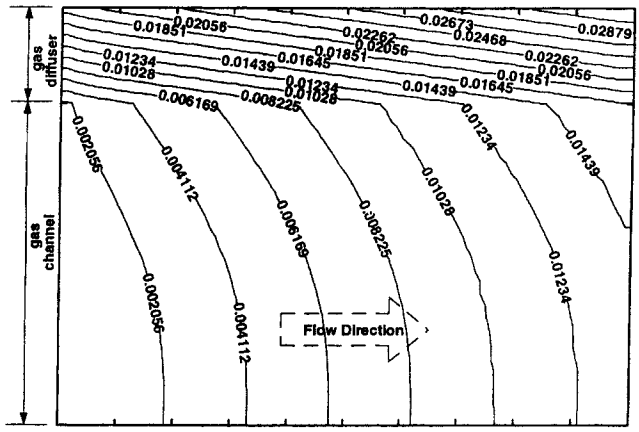

Figure 10. Water vapor mole fraction in the cathode gas channel-gas diffuser domain.

For $I_{avg} = 1.08 \times 10^3$ A/m^2, $U_i = 0.35$ m/s, $T = 353$ K (isothermal case), $X_{w,i} = 0$.

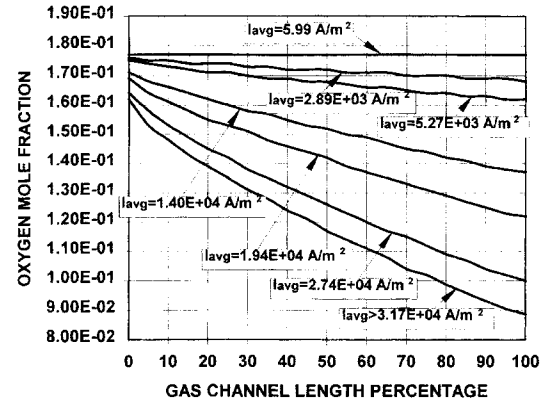

Figure 12. Oxygen mole fraction distribution along the gas channel-gas diffuser interface, for different cell operating current densities.

$U_i = 0.35$ m/s, $T = 353$ K (isothermal case), $X_{w,i} = 0.1579$ (100% humidity), $\epsilon = 0.40$.

mole fraction at the inlet and the average oxygen mole fraction difference between exit and inlet.

Water vapor mole fraction field in the cathode gas channel-gas diffuser coupled domain

Figures 10 and 11 show the water vapor mole fraction in the cathode gas channel-gas-diffuser coupled domain for two different current densities. In both cases, air entering the gas channel is completely dry. It is assumed that the water produced at the cathode gas diffuser-catalyst layer interface is in vapor state. The maximum water vapor mole fraction is the one corresponding to the water saturation pressure. If more water vapor is produced, it will condense. In Figure 10, since the current density is relatively small, the reaction rate is small as well and the water partial pressure is smaller than the water saturation pressure. In Figure 11, more water vapor is produced and the maximum water vapor mole fraction corresponds to the saturation pressure (100% humidity). In both cases, $X_w^{sat} = 0.1579$ corresponds to a temperature of 353 K and a pressure of 3 atm in the cathode.

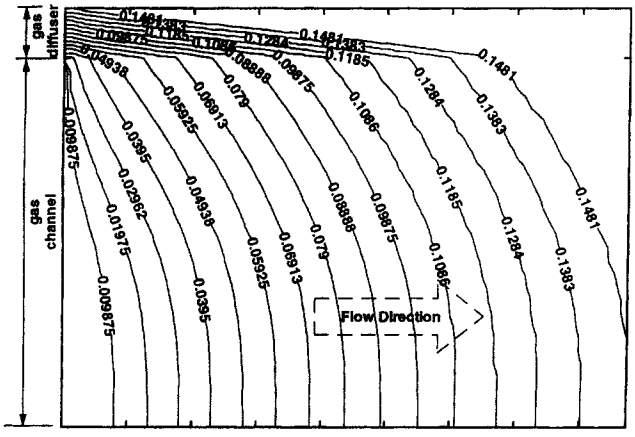

Figure 11. Water vapor mole fraction in the cathode gas channel-gas diffuser domain.

For $I_{avg} = 3.18 \times 10^4$ A/m^2, $U_i = 0.35$ m/s, $T = 353$ K (isothermal case), $X_{w,i} = 0$.

Oxygen mole fraction distribution as a function of the fuel cell operating current density

Most of the mathematical models for PEM fuel cells use oxygen mole fraction or partial pressure distributions along the cathode gas channel-gas-diffuser interface as input data. These "guessed" or *a priori* prescribed distributions may eventually affect the computed values of the operating current density. The present mathematical model enables us to solve the transport equations in the coupled gas channel-gas-diffuser domain; therefore, the oxygen mole fraction is *calculated*, not *prescribed*. Figure 12 presents the computed oxygen mole fraction distributions at the interface between the cathode gas channel and gas diffuser for the base case conditions and different operating current densities. For higher operating current densities, these distributions are clearly nonlinear, as assumed in other models. For the base case conditions and operating current densities higher than 3.17×10^4 A/m^2, the oxygen mole fraction distribution remains almost unchanged at this interface, which shows that limiting current density is approached.

Current density distribution at the membrane-cathode catalyst layer as a function of the fuel cell operating current density

If the operating current density was an input datum and the distribution of the oxygen mole fraction at the cathode gas channel-gas diffuser was not prescribed before performing the computations, it would be unclear how the current density distribution could be found. Even though the operating current density is the average of the current density distribution at the membrane-cathode catalyst layer interface, the knowledge of the former one is not sufficient to determine the latter one. Therefore, in the present formulation we used the total electrode overpotential as an input datum to find the operating current density, the current density distribution, and the oxygen mole fraction distribution. This was possible, since there is a one-to-one relationship between the cell overpotential and the cell voltage. It is true that for a certain regime, the total electrode overpotential is not known *a priori*. Therefore, one has to calculate the operating current

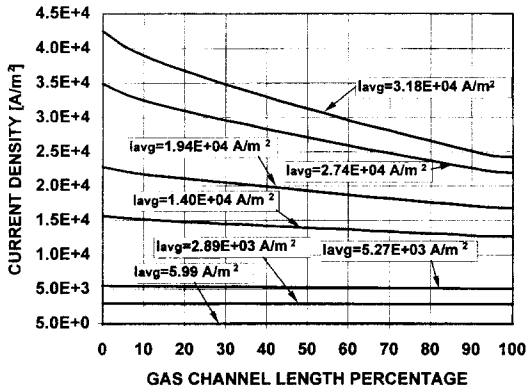

Figure 13 The current density distribution along the membrane-catalyst layer interface, for different cell operating current densities.

$U_i = 0.35$ m/s, $T = 353$ K (isothermal case), $X_{w,i} = 0.1579$ (100% humidity), $\epsilon = 0.40$.

density-cell voltage curve for different regimes from zero current density until the limiting current density is achieved, and after that interpolate for the desired regime. Figure 13 shows the current density distribution at the membrane-cathode catalyst layer interface, for the base case and the oxygen mole fraction distributions in Figure 12.

Membrane liquid water velocity field

The transport of liquid water in the porous membrane is due to the superposition of certain effects: the pressure field, the proton drag, friction with the pore walls, and water concentration field. The pressure field and the proton drag have opposite effects. Since water is produced at the cathode, the back diffusion has the same effect on the water transport as the pressure field. At lower current densities, when the proton drag is less important than the pressure field, water will be transported from cathode to anode. When the current density becomes more significant, water will move against the pressure field, from anode to cathode. Since the current density is higher towards the gas channel entries (see Figure 13), the effect of the proton drag will be also more important in that part of the membrane. As a consequence, the water velocity (specific discharge) field in the membrane will be not uniform along the y direction (see Figure 2). Therefore, there will be a range of the intermediate overall effect on the water transport, when water will move from the anode to the cathode in the membrane region closer to the gas channel entries and in the opposite direction in the rest of membrane. Figures 14a, 14b and 14c present three different regimes of the membrane water transport. For the base case conditions and operating current densities lower than 850 A/m^2, water will be transported from cathode to anode (Figure 14a). For currents higher than 900 A/m^2, it will be transported in the op-

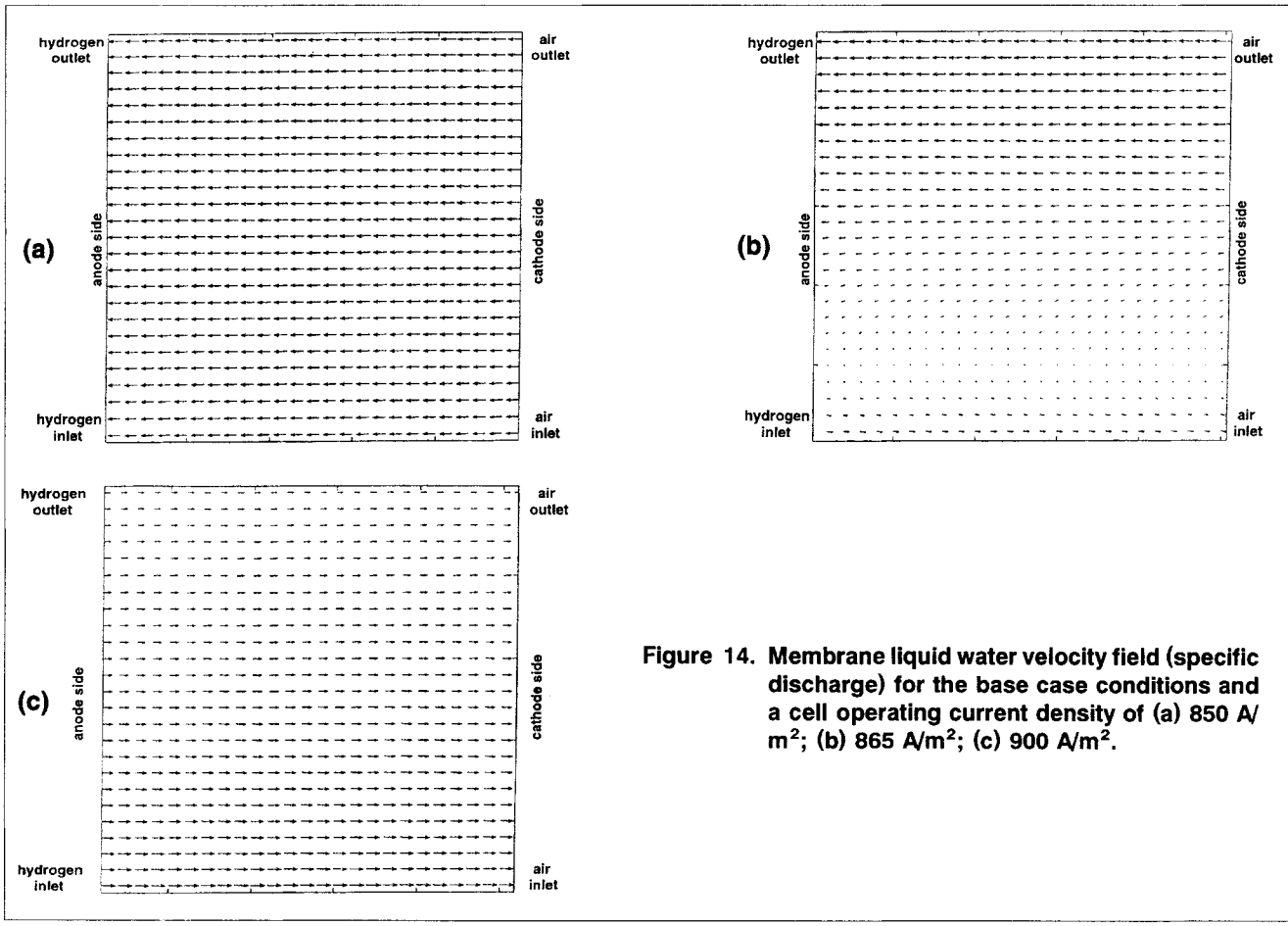

Figure 14. Membrane liquid water velocity field (specific discharge) for the base case conditions and a cell operating current density of (a) 850 A/m^2; (b) 865 A/m^2; (c) 900 A/m^2.

posite direction (Figure 14c). In between these approximate limits, the picture will be similar to Figure 14b.

Conclusion

The mathematical model presented here enables prediction of phenomena in the entire fuel cell sandwich, including the gas channels. The input data are only those parameters that can be controlled in real fuel cell applications. No assumptions are necessary for the distribution of the species concentrations or current density, as they are assumed in other fuel cell models available in the literature. The computed oxygen mole fraction along the gas channel-gas-diffuser interface and the current density along the membrane-catalyst layer interface do not present linear distributions, as are assumed in other works. The oxygen mole fraction field is also presented in the coupled gas channel-gas-diffuser domain. The computed fuel cell performances are realistic.

Notation

aj_0^{ref} = reference exchange current density times area, $A \cdot m^{-3}$
c = molar concentration, $mol \cdot m^{-3}$
D = gas channel width, m
E = thermodynamic open circuit potential, V
I_{avg} = operating cell current density, $A \cdot m^{-2}$
k_Φ = electrokinetic permeability, m^2
M = molecular mass, $kg \cdot kmol^{-1}$
n = number of electrons participating in reaction
p = pressure, Pa
Pe = Peclet number
Pr = Prandtl number
Q = heat source, $W \cdot m^{-2}$
$r^{(2)}$ = coefficient in the generalized Darcy's equation
Re = Reynolds number
S = entropy, $J \cdot kg^{-1} \cdot K^{-1}$
S = source term of the generalized transport equation
T = temperature, K
u, v = velocity components, $m \cdot s^{-1}$
x, y = coordinates, m

Greek letters

α = transfer coefficient
Γ = diffusion coefficient of the generalized transport equation
η = total electrode overpotential, V
λ = membrane water content, mol H_2O/mol SO_3^-
ρ = density, $kg \cdot m^{-3}$
μ = viscosity, $kg \cdot m^{-1} \cdot s^{-1}$
ξ = stoichiometric ratio

Superscripts

$-$ = nondimensionalized variable
ref = reference

Subscripts

a = anode
A, B = components
avg = average
c = cathode
ch = channel
cl = catalyst layer
cr = critical
e = exit
eff = effective
f = related to the sulfonic acid ions
H^+ = related to the hydrogen protons
H_2 = related to the hydrogen molecule
i = inlet
inter = interface
l = liquid
O_2 = related to the oxygen molecule
pm = porous medium
w = wall or related to water
x, y = directions
$+$ = cathode

Literature Cited

Amphlett, J. C., R. M. Baumert, R. F. Mann, B. A. Peppley, and P. R. Roberge, "Performance Modeling of the Ballard Mark IV Solid Polymer Electrolyte Fuel Cell," *J. Electrochem. Soc.*, **142**, 1 (1995).

Beavers, G. S., and D. D. Joseph, "Boundary Conditions at a Naturally Permeable Wall," *J. of Fluid Mechanics*, **30**, 197 (1967).

Beavers, G. S., E. M. Sparrow, and R. A. Magnuson, "Experiments on Coupled Parallel Flows in a Channel and a Bounding Porous Medium," *Trans. ASME, J. Basic Eng.*, **30**, 843 (1970).

Bernardi, D. M., and M. W. Verbrugge, "Mathematical Model of a Gas Electrode Bonded to a Polymer Electrolyte," *AIChE J.*, **37**, 1151 (1991).

Bernardi, D. M., and M. W. Verbrugge, "A Mathematical Model of the Solid-Polymer-Electrolyte Fuel Cell," *J. Electrochem. Soc.*, **139**, 2477 (1992).

Bird, R. B., W. Stewart, and E. N. Lightfoot, *Transport Phenomena*, Wiley, New York (1960).

Bockris, J. O'., and S. Srinivasan, *Fuel Cells: Their Electrochemistry*, McGraw-Hill, New York.

Dagan, G., "The Generalization of Darcy's Law for Nonuniform Flows," *Water Resour. Res.*, **15**, 1 (1979).

Dagan, G., *Flow and Transport in Porous Formations*, Springer-Verlag, Berlin (1989).

Fuller, T. F., and J. Newman, "Water and Thermal Management in Solid-Polymer-Electrolyte Fuel Cells," *J. Electrochem. Soc.*, **5**, 1218 (1993).

Gurau, V., "Two Dimensional Mathematical Model and Numerical Simulation of the Transport Processes and Cell Performance of H_2-O_2 Proton Exchange Membrane Fuel Cells," PhD Thesis, Univ. of Miami, Coral Gables, FL (1998).

Kakac, S., and Y. Yener, *Convective Heat Transfer*, 2nd ed., CRC Press, Boca Raton, FL (1994).

Nguyen, T. V., and R. E. White, "A Water and Heat Management Model for Proton-Exchange-Membrane Fuel Cells," *J. Electrochem. Soc.*, **140**, 2178 (1993).

Parthasarathy, A., S. Srinivasan, and A. J. Appleby, "Temperature Dependence of the Electrode Kinetics of Oxygen Reduction at the Platinium/Nafion Interface—A Microelectrode Investigation," *J. Electrochem. Soc.*, **139**, 2530 (1992).

Patankar, S. V., *Numerical Heat Transfer and Fluid Flow*, Hemisphere, New York (1980).

Ridge, S. J., R. E. White, Y. Tsou, R. N. Beaver, and G. A. Eisman, "Oxygen Reduction in a Proton Exchange Membrane Test Cell," *J. Electrochem. Soc.*, **136**, 1902 (1989).

Singh, D., D. M. Lu, and N. Djilali, "Numerical Analysis of Transport Processes in Proton Exchange Membrane Fuel Cells," *Proc. of Int. Energy and Environ. Symp.*, Karadeniz Technical Univ., Trabzon, Turkey, p. 615 (1996).

Slattery, J. C., and R. B. Bird, "Calculation of the Diffusion Coefficient of Dilute Gases and of the Self-Diffusion Coefficient of Dense Gases," *AIChE J.*, **4**(2), 137 (1958).

Springer, T. E., T. A. Zawodinski, and S. Gottesfeld, "Polymer Electrolyte Fuel Cell Model," *J. Electrochem. Soc.*, **136**, 2334 (1991).

Ticianelli, E. A., C. R. Derouin, and S. Srinivasan, "Localization of Platinum in Low Catalyst Loading Electrodes to Attain High Power Densities in SRE Fuel Cells," *J. Electroanal. Chem.*, **251**, 275 (1988).

Verbrugge, M. W., and R. F. Hill, "Ion and Solvent Transport in Ion-Exchange Membranes," *J. Electrochem. Soc.*, **137**, 886 (1990).

Verbrugge, M. W., and R. F. Hill, "Analysis of Promising Perfluorosulfonic Acid Membranes for Fuel-Cell Electrolytes," *J. Electrochem. Soc.*, **137**, 3770 (1990).

Manuscript received Feb. 12, 1998, and revision received Aug. 27, 1998.